Phys. Biol. **7** (2010) 016001 (14pp) doi:10.1088/1478-3975/7/1/016001

Molecular electroporation and the transduction of oligoarginines

Kevin Cahill

Biophysics Group, Department of Physics & Astronomy, University of New Mexico, Albuquerque, NM 87131, USA

E-mail: cahill@unm.edu

Received 17 November 2008
Accepted for publication 27 October 2009
Published 11 December 2009
Online at stacks.iop.org/PhysBio/7/016001

Abstract

Certain short polycations, such as TAT and polyarginine, rapidly pass through the plasma membranes of mammalian cells by an unknown mechanism called transduction as well as by endocytosis and macropinocytosis. These cell-penetrating peptides (CPPs) promise to be medically useful when fused to biologically active peptides. I offer a simple model in which one or more CPPs and the phosphatidylserines of the inner leaflet form a kind of capacitor with a voltage in excess of about 200 mV, high enough to create a molecular electropore. The model is consistent with an empirical upper limit on the cargo peptide of 40–60 amino acids and with experimental data on how the transduction of a polyarginine-fluorophore into mouse C_2C_{12} myoblasts depends on the number of arginines in the CPP and on the CPP concentration. The model makes three testable predictions.

1. Cell-penetrating peptides

In 1988, two groups [1, 2] working on HIV reported that the trans-activating transcriptional activator (TAT) of HIV-1 can cross cell membranes. The engine driving this 86-aa cell-penetrating peptide (CPP) is its residues 48–57 GRKKRRQRRR which carry a charge of $+8e$. Other CPPs were soon found. Antp (aka Penetratin, PEN) is residues 43–58 RQIKIWFQNRRMKWKK of antennapedia, a homeodomain of the fly; it carries a charge of $+7e$. The polyarginine $(\mathrm{Arg})_n$ carries charge $+ne$, where often $n = 7$, 8 or 9. Other CPPs have been discovered (VP22) or synthesized (transportan). The structural protein VP22 of the tegument of herpes simplex virus type 1 (HSV-1) has charge $+15e$. Transportan GWTLNSAGYLLG-K-INLKALAALAKKIL-amide is a chimeric peptide constructed from the 12 N-terminal residues of galanin in the N-terminus with the 14-residue sequence of mastoparan and a connecting lysine [3]. With its terminal amide group, its charge is $+5e$.

These and other short, positively charged peptides can penetrate the plasma membranes of live cells and can tow along with them cargoes that greatly exceed the 600 Da restriction barrier. They are promising therapeutic tools when towing cleverly chosen peptide cargoes of from 8 to 33 amino acids [4–16].

Many early experiments on CPPs were wrong because the cells were fixed or insufficiently washed. Even careful experiments sometimes have yielded inconsistent results—in part because fluorescence varies with the (sub)cellular conditions and the fluorophores [17].

Yet some clarity is emerging: TAT carries cargoes across cell membranes with high efficiency by at least two functionally distinct mechanisms according to whether the cargo is big or small [18]. Big cargoes, such as proteins or quantum dots, enter via caveolae endocytosis and macropinocytosis [19, 20], and relatively few escape the cytoplasmic vesicles in which they then are trapped [18].

Small cargoes, such as peptides of fewer than 30–40 amino acids, enter both slowly by endocytosis and rapidly by transduction with direct access to the cytosol, an unknown mechanism that uses the membrane potential [18, 21–24]. Peptides fused to TAT enter cells within seconds [25].

It remains unclear how big cargoes aided by several CPPs enter cells [26]. For instance, superparamagnetic nanoparticles encased in aminated dextran and attached to 45 tat peptides are thought to enter cells by adsorptive endocytosis[27–29] but they do enter slowly at 4°C [30].

This paper is exclusively about how polycationic cell-penetrating peptides, specifically oligoarginines, transduce small cargoes directly into the cytosol. Section 2 recalls some

basic facts about plasma membranes, and section 3 explains why ions do not normally pass through plasma membranes. Section 4 describes a simple model of the transduction of CPPs in which electroporation and phosphatidylserine play key roles. In this model, one or more positively charged CPPs on the outer leaflet and the negatively charged PSs under it on the inner leaflet form a kind of capacitor, which enhances the membrane potential to a voltage of more than about 200 mV, which is sufficient to create an electropore. Section 5 shows that the model is consistent with an empirical upper limit on the cargo of 40–60 amino acids and with measurements made by Tünnemann *et al* [31] on the fraction of mouse myoblasts transduced by polyarginines carrying fluorophores of 400 Da. Section 6 tells how to test three predictions of the model. The paper ends with a short summary in section 7.

2. Mammalian plasma membranes

The plasma membrane of a mammalian cell is a lipid bilayer that is 4 or 5 nm thick. Of the four main phospholipids in it, three—phosphatidylethanolamine (PE), phosphatidylcholine (PC) and sphingomyelin (SM)—are neutral, and one, phosphatidylserine (PS), is negatively charged. In live cells, PE and PS are mostly in the cytosolic layer, and PC and SM in the outer layer [32, 33]. Aminophospholipid translocase (flippase) moves PE and PS to the inner layer; floppase slowly moves all phospholipids to the outer layer [32].

Incidentally, the surfaces of bacteria are different. The cell wall of a Gram-positive bacterium (e.g. *Streptococcus* or *Staphylococcus*) is covered with negatively charged teichoic acids; the outer leaflet of the outer membrane of a Gram-negative bacterium (e.g. *E. coli* or *Salmonellum*) is tiled by negatively charged lipopolysaccharides (LPS) held together by divalent cations [34, 35].

Glycolipids make up about 5% of the lipid molecules of the outer layer of a mammalian plasma membrane where they may form lipid rafts. Their hydrocarbon tails normally are saturated. Instead of a modified phosphate group, they are decorated with galactose, glucose, GalNAc = *N*-acetylgalactosamine, and other sugars. The most complex glycolipids—the gangliosides—have negatively charged sialic acid (NANA) groups. Incidentally, cholera toxin binds to and enters cells that display the G_{M1} ganglioside [33].

A living cell maintains an electrostatic potential of between 20 and 120 mV across its plasma membrane. The electric field E within the membrane points into the cell and is huge, about 15 mV nm^{-1} or 1.5×10^7 V m^{-1} if the potential difference is 60 mV across a membrane of 4 nm. Conventionally, one reports membrane potentials as the electric potential inside the cell minus that outside, so that here $\Delta V = -60$ mV. Near but outside the membrane, this electric field falls off exponentially $E(r) = E\exp(-r/D_\ell)$ with the ratio of the distance r from the membrane to the Debye length D_ℓ, which is of the order of a nanometer. The rapid entry of TAT fused to peptides is frustrated only by agents that destroy the electric field E [18], which applies a force qE to a CPP of charge q.

Most of the phospholipids of the outer leaflet of the plasma membrane are neutral PCs & SMs. They vastly outnumber the negatively charged gangliosides, which are a subset of the glycolipids, which themselves amount only to 5% of the outer layer. Imagine now that CPP-cargo molecules are in the extracellular environment. Many of them will be pinned down by the electric field $E(r)$ just outside the membrane, their positively charged side chains interacting with the negative phosphate groups of neutral dipolar PC & SM head groups [23]. (Other CPP–cargo molecules will stick to negatively charged gangliosides and to glycosaminoglycans (GAGs) attached to transmembrane proteoglycans (PGs); these slowly will be endocytosed. PGs with heparan-sulfate GAGs are needed for TAT-protein endocytosis [36]. A more detailed analysis than that of this work might model the effect of these anionic matrix compounds upon transduction.) It is crucial that the dipolar PC & SM head groups are neutral and so do not cancel or reduce the positive electric charge of a CPP–cargo molecule. The net positive charge of a CPP–cargo molecule and the negatively charged PSs under it on the inner leaflet form a kind of capacitor. This is the starting point for the model described in section 4.

3. The problem

The relative permittivity $\epsilon_\ell \approx 2$ of the hydrocarbons of a lipid bilayer is much less than that of water $\epsilon_w \approx 80$. Thus, the difference $\Delta E_{w\to\ell}$ in the electrostatic energy of an ion of charge q and effective radius a in the bilayer and in water [37] is

$$\Delta E_{w\to\ell} = \frac{q^2}{8\pi\epsilon_0 a}\left(\frac{1}{\epsilon_\ell} - \frac{1}{\epsilon_w}\right) \tag{1}$$

or 3.5 eV if the ion's charge is that of the proton and its radius is $a = 1$ Å. This energy barrier is far larger than the 0.06 eV gained when a unit charge crosses a 60 mV phospholipid bilayer. Thus, an ion will not cross a cell's plasma membrane unless a transporter or a channel facilitates (and regulates) its passage.

The electrostatics of a cationic polypeptide such as TAT or polyarginine are more complex than for an ion. I will model the CPP and its cargo in water as a sphere with its positive charges on its surface. The density of a protein of mass M kDa is estimated [38] to be

$$\rho(M) = (0.8491 + 0.0873\,\mathrm{e}^{-M/13})\ \text{kDa nm}^{-3}. \tag{2}$$

A CPP–cargo complex would not be expected to fold as densely as a natural globular protein, and so for it the estimate $\rho(M)$ is something of an upper bound. The radius r of a putative sphere consisting of M kDa of CPP and cargo then would be

$$r \gtrsim \left(\frac{3}{4\pi}\frac{M}{\rho(M)}\right)^{1/3}\text{nm}. \tag{3}$$

For instance, a CPP of N arginines and a tiny fluorophore cargo of 400 Da has a mass of $M_N = 0.1562N + 0.4$ kDa, and so its radius would satisfy

$$r \gtrsim \left(\frac{3}{4\pi}\frac{M_N}{\rho(M_N)}\right)^{1/3}\text{nm} \tag{4}$$

Table 1. The radius r of a CPP–cargo molecule of N arginines and a cargo of 400 Da, its change in electrostatic energy $\Delta E_{w,\ell}$ when transferred from water to hydrocarbon (equation (14)), and the short-distance correction $\Delta E_{\rm SDC}$ (equation (15)). Distances are in nm and energies in eV.

N	r	$\Delta E_{w,\ell}$	$\Delta E_{\rm sdc}$
5	0.67	4.61	3.90
6	0.70	6.39	4.68
7	0.73	8.41	5.46
8	0.75	10.64	6.24
9	0.78	13.06	7.02
10	0.80	15.68	7.80
11	0.82	18.48	8.58
12	0.84	21.44	9.36

or $r = 0.75$ nm for $N = 8$ arginines. The lower bounds on the radii for $N = 5$–12 are listed in column 2 of table 1.

For larger cargoes of $A = 50$–100 amino acids of 130 Da each, the lower bounds on the radii range from 1.25 to 1.59 nm. (In what follows, A will represent the number of amino acids in the cargo or the mass of the cargo in Daltons divided by 130 Da.) Adding another 0.8 nm for the PC/SM head groups would extend these lower bounds on the radii to 2.05–2.39 nm.

If the CPP–cargo molecule were a charged conducting sphere of radius r and charge q, then its electrostatic energy in water would be

$$E(N, A, q, w) = \frac{q^2}{8\pi\epsilon_0\epsilon_w r}. \tag{5}$$

This term neglects the short-distance detail of the electric field near the q/e positive unit charges e of the CPP–cargo molecule. So a short-distance correction term

$$E_{\rm sdc}(a, q, w) = \frac{qe}{8\pi\epsilon_0\epsilon_w a} \tag{6}$$

proportional to q must be added to $E(N, A, q, w)$. The short distance a is a parameter, which may be taken to be a few Å because the term $E_{\rm sdc}$ is a correction to be added to $E(N, A, q, w)$ and not the entire electrostatic energy.

The electrostatic field of the cell attracts the CPP–cargo molecule to the surface of the cell. While on the outer leaflet of the plasma membrane, the electrostatic energy of the CPP–cargo molecule and its short-distance correction are no longer given by their values in water equations (5) and (6) but instead are those appropriate to the interface between water and lipid:

$$E(N, A, q, w\ell) = \frac{q^2}{8\pi\epsilon_0\bar{\epsilon}r} \tag{7}$$

and

$$E_{\rm sdc}(a, q, w\ell) = \frac{qe}{8\pi\epsilon_0\bar{\epsilon}a} \tag{8}$$

where $\bar{\epsilon}$ is the mean permittivity

$$\bar{\epsilon} = \tfrac{1}{2}(\epsilon_w + \epsilon_\ell). \tag{9}$$

The CPP–cargo molecule enters the lipid bilayer as a CPP–cargo–PC/SM complex with the phosphate groups of the PC and SM of the outer leaflet bound to the positively charged guanidinium and amine groups of the CPP [23]. The positive charges of the phosphocholine groups of PC and SM are about $d = 5$ Å from their phosphate groups [39]. The binding of PC and SM therefore approximately increases the effective radius of the charged sphere to $r_m \approx r + d$. The electrostatic energy of this complex in the hydrocarbon tails of the lipid bilayer then is

$$E(N, A, q, \ell) \approx \frac{q^2}{8\pi\epsilon_0\epsilon_\ell(r + d)} \tag{10}$$

apart from a short-distance correction factor

$$E_{\rm sdc}(a, q, \ell) = \frac{qe}{8\pi\epsilon_0\epsilon_\ell a} \tag{11}$$

similar to (6).

Apart from correction terms, the electrostatic energy penalty when the CPP–cargo molecule enters the lipid bilayer from water as a CPP–cargo–PC/SM complex is the difference

$$\begin{aligned}\Delta E^0_{w,\ell}(N, A, q) &\approx E(N, A, q, \ell) - E(N, A, q, w\ell)\\ &\approx \frac{q^2}{8\pi\epsilon_0\epsilon_\ell(r + d)}\left(1 - \frac{r + d}{r}\frac{\epsilon_\ell}{\bar{\epsilon}}\right).\end{aligned} \tag{12}$$

Because the thickness $\ell = 4.4$ nm of the lipid bilayer is at most a few times the diameter of the CPP–cargo–PC/SM complex, we also must include the Parsegian correction [37]

$$\Delta E_P = -\frac{q^2}{4\pi\epsilon_0\epsilon_\ell\ell}\ln\left(\frac{2\epsilon_w}{\epsilon_w + \epsilon_\ell}\right) \tag{13}$$

which holds when a uniformly charged sphere is inserted into the middle of a lipid layer of thickness ℓ. The sum of the water-to-lipid energy (12) and Parsegian's correction (13) is

$$\Delta E_{w,\ell}(N, A, q) = \Delta E^0_{w,\ell}(N, A, q) + \Delta E_P. \tag{14}$$

The energy $\Delta E_{w,\ell}(N, A, q)$ is listed in column 3 of table 1 for a CPP of $N = 5$–12 arginines towing a fluorophore cargo of 400 Da with $d = 0.5$ nm.

The short-distance correction terms augment this penalty by

$$\begin{aligned}\Delta E_{\rm sdc}(a, q) &= E_{\rm sdc}(a, q, \ell) - E_{\rm sdc}(a, q, w)\\ &= \frac{qe}{8\pi\epsilon_0\epsilon_\ell a}\left(1 - \frac{\epsilon_\ell}{\epsilon_w}\right)\end{aligned} \tag{15}$$

and do not require Parsegian's correction because they are short-distance effects. This short-distance correction $\Delta E_{\rm sdc}$ is listed in column 4 of table 1 for CPPs of $N = 5$–12 arginines and a representative value of $a = 4.5$ Å for the short-distance parameter.

The net electrostatic energy penalty when the CPP–cargo molecule enters the lipid bilayer from water as a CPP–cargo–PC/SM complex is then the sum of (12), (13) and (15):

$$\Delta E_{w\to\ell} = \Delta E^0_{w,\ell} + \Delta E_P + \Delta E_{\rm sdc}. \tag{16}$$

A CPP of eight arginines carrying a fluorophore of 400 Da ($A = 3 \approx 400/130$) has a radius r of 0.75 nm, and with $a = 4.5$ Å, the change (16) in its electrostatic energy on going from water to lipid is

$$\Delta E_{w\to\ell} \approx 16.9\ \text{eV}. \tag{17}$$

This energy barrier is 35 times bigger than the energy 0.48 eV that it gains by crossing a potential difference of 60 mV. So how and why does it cross?

4. The model

My answer is that one (or more) oligoarginines and the phosphatidylserines (PSs) of the inner leaflet together with their counterions form a kind of capacitor with an electric field strong enough to form a reversible pore in the plasma membrane. The transmembrane potential is the sum of three terms—the resting transmembrane potential $\Delta V_{\rm cell}$ of the cell in the absence of CPPs, the transmembrane potential $\Delta V_{\rm CPP}$ due to an oligoarginine and the transmembrane potential $\Delta V_{\rm NaCl}$ due to the counterions of the extracellular medium:

$$\Delta V = \Delta V_{\rm cell} + \Delta V_{\rm CPP} + \Delta V_{\rm NaCl}. \tag{18}$$

The resting transmembrane potential $\Delta V_{\rm cell}$ of the cell varies between about 20 mV to more than 70 mV, depending upon the type of cell. Ideally, it is measured experimentally.

My model is based upon several considerations, which I discuss in turn in this section. The first subsection describes the basic facts about electroporation. The second subsection presents the electric potential V due to a charge in the extracellular medium; the derivation of that potential is in an appendix. This potential implies that charges on opposite sides of the lipid bilayer are effectively decoupled, which simplifies the subsequent analysis. The third subsection describes a Monte Carlo simulation of the response of the phosphatidylserines of the inner leaflet to an oligoarginine interacting with the phosphate groups of the outer leaflet. To a very good approximation, the PSs are distributed uniformly and randomly because they are nearly decoupled from the oligoarginine. The fourth subsection uses the potential V to compute the contribution $\Delta V_{\rm CPP}$ of an oligoarginine to the transmembrane potential. The fifth subsection describes a Monte Carlo simulation of the effect $\Delta V_{\rm NaCl}$ of the sodium and chloride ions in the extracellular medium upon the transmembrane potential. The section ends with a summary of the model.

4.1. Electroporation

Electroporation is the formation of pores in membranes by an electric field. Depending on the duration of the field and the type of cell, an electric potential difference across a cell's plasma membrane in excess of about 200 mV will create pores. There are two main components to the energy of a pore. The first is the line energy $2\pi r\gamma$ due to the linear tension γ, which is of the order of 10^{-11} J m^{-1}. The second is the electrical energy $-0.5\Delta C\pi r^2(\Delta V)^2$ in which ΔV is the voltage across the membrane and $\Delta C = C_w - C_\ell$ is the difference between the specific capacity per unit area $C_w = \epsilon_w\epsilon_0/t$ of the water-filled pore and $C_\ell = \epsilon_\ell\epsilon_0/t$ of the pore-free membrane of thickness t. There also is a small term due to the surface tension Σ of the plasma membrane of the cell, but this term usually is negligible since Σ is of the order of 2.5×10^{-6} J m^{-2} [40]. The energy of the pore in a plasma membrane is then [41–45]

$$E(r) = 2\pi r\gamma - \pi r^2\Sigma - \tfrac{1}{2}\pi r^2\Delta C(\Delta V)^2. \tag{19}$$

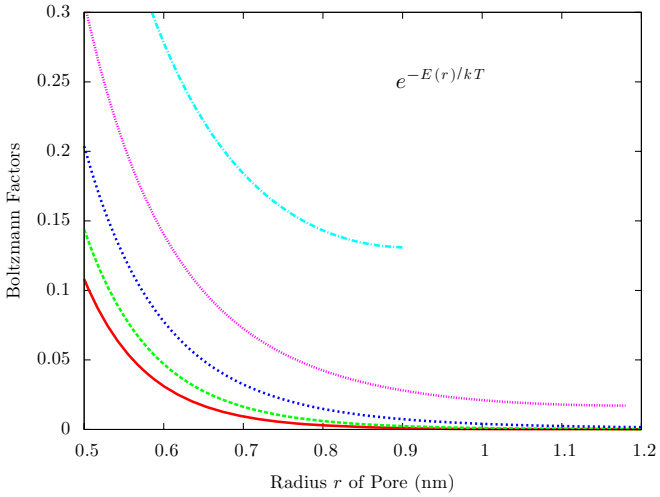

Figure 1. The Boltzmann factor $e^{-E(r)/kT}$ ($\times 100$) for energy $E(r)$ (equation (19)) is plotted against the radius r of the pore up to the critical radius r_c (equation (21)) for the transmembrane voltage $\Delta V = -200$ (solid red), -250 (dashes green), -300 (dots blue), -350 (dots magenta) and -400 mV (dash-dot cyan).

This energy has a maximum of

$$E(r_c) = \frac{\pi\gamma^2}{\Sigma + \frac{1}{2}\Delta C(\Delta V)^2} \approx \frac{2\pi\gamma^2}{\Delta C(\Delta V)^2} \tag{20}$$

at the critical radius

$$r_c = \frac{\gamma}{\Sigma + \frac{1}{2}\Delta C\,(\Delta V)^2} \approx \frac{2\gamma}{\Delta C\,(\Delta V)^2}. \tag{21}$$

In figure 1, the Boltzmann factor $e^{-E(r)/(kT)}$ ($\times 100$) is plotted as a function of the radius r of the pore up to r_c for various transmembrane voltages from -200 (solid, red) to -400 mV (dot-dash, cyan). Clearly, the chance of a pore forming rises steeply with the magnitude of the voltage and falls with the radius of the pore.

If the transmembrane potential ΔV is turned off before the radius of the pore reaches r_c, then the radius r of the pore usually shrinks quickly (well within 1 ms [42]) to a radius so small as to virtually shut down the conductivity of the pore. This rapid closure occurs because in (19) the energy $2\pi r\gamma$ dominates over $-\pi r^2\Sigma$, the surface tension Σ being negligible. Such a pore is said to be reversible. But if ΔV remains on when r exceeds the critical radius r_c, then the pore usually will grow and lyse the cell; such a pore is said to be irreversible.

Formula (21) provides an upper limit on the radius of a reversible pore. This upper limit drops with the square of the transmembrane voltage ΔV from $r_c = 3.6$ nm for $\Delta V = -200$ mV, to 1.6 nm for $\Delta V = -300$ and to 0.9 nm for $\Delta V = -400$ mV.

The time t_ℓ for a pore's radius to reach the critical radius r_c is the time to lysis; it varies greatly and apparently randomly even within cells of a given kind. In erythrocytes, its mean value drops by nearly an order of magnitude with each increase of 100 mV in the transmembrane potential [42] and is about a fifth of a second when $\Delta V = -300$ mV.

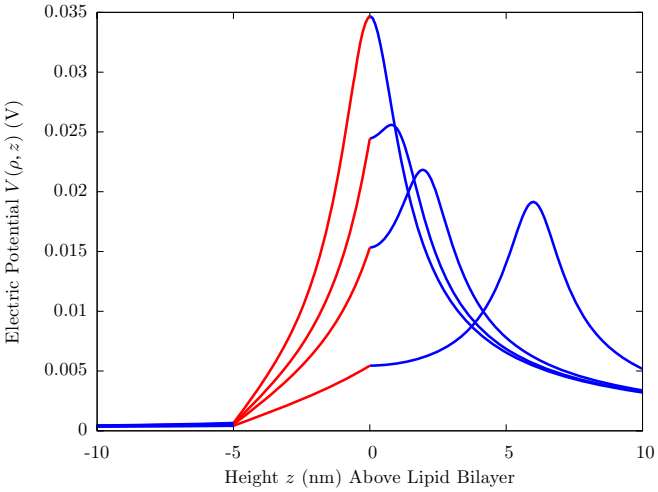

Figure 2. The electric potential $V(\rho, z)$ from (22)–(25) in volts for $\rho = 1$ nm as a function of the height z (nm) above the phospholipid bilayer for a unit charge $q = |e|$ at $(\rho, z) = (0, 0)$ (top curve), $(0, 1)$ (second curve), $(0, 2)$ (third curve) and $(0, 6)$ nm (bottom curve). The lipid bilayer extends from $z = 0$ to $z = -5$ nm, and the cytosol lies below $z = -5$ nm. The relative permittivities were taken to be $\epsilon_w = \epsilon_c = 80$ and $\epsilon_\ell = 2$.

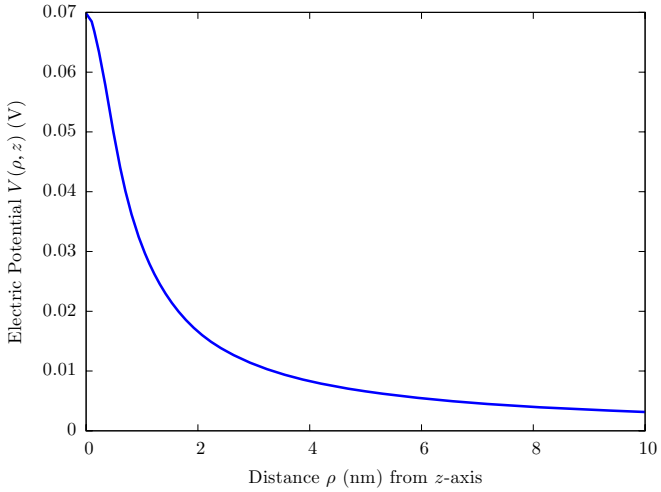

Figure 3. The electric potential $V(\rho, z)$ from (24) in volts for $0 \leqslant \rho \leqslant 10$ nm at a height $z = 0.5$ (nm) above the phospholipid bilayer for a unit charge $q = |e|$ at $(\rho, z) = (0, 0)$ nm. Same geometry and parameters as in figure 2.

In the present model, however, the potential is imposed by the CPP and the PSs, and so when that potential causes a pore to form, the CPP and its cargo may enter the cell through the pore that they have formed, and once they do, the potential drops to its normal resting value, usually less than -100 mV, and the pore virtually closes within 1 ms.

The oligoarginine(s) on the interface between the outer leaflet and the extra-cellular environment, the negatively charged head groups of the PSs below them in inner leaflet, and their counterions create an electric field and a transmembrane potential ΔV. The chance of this potential forming a pore of radius r is proportional to the Boltzmann factor $e^{-E(r)/(kT)}$, which is plotted in figure 1. The higher the potential ΔV and the narrower the pore, the greater the chance of pore formation.

4.2. The potential of an external charge

As shown in appendix A, the electrostatic potential in the lipid bilayer $V_\ell(\rho, z)$ due to a charge q at the point $(0, 0, h)$ on the z-axis, a height h above the interface between the lipid bilayer and the extra-cellular environment is

$$V_\ell(\rho, z) = \frac{q}{4\pi\epsilon_0\epsilon_{w\ell}} \sum_{n=0}^{\infty} (pp')^n \left(\frac{1}{\sqrt{\rho^2 + (z - 2nt - h)^2}} - \frac{p'}{\sqrt{\rho^2 + (z + 2(n+1)t + h)^2}} \right) \tag{22}$$

in which t is the thickness of the lipid bilayer, $\epsilon_{w\ell} = (\epsilon_w + \epsilon_\ell)/2$ is the average of the relative permittivity of the extra-cellular fluid ϵ_w and that of the lipid bilayer ϵ_ℓ, and p and p' are the ratios

$$p = \frac{\epsilon_w - \epsilon_\ell}{\epsilon_w + \epsilon_\ell} \qquad \text{and} \qquad p' = \frac{\epsilon_c - \epsilon_\ell}{\epsilon_c + \epsilon_\ell} \tag{23}$$

which lie between 0 and 1, ϵ_c being the relative permittivity of the cytosol. The potential in the extra-cellular medium is

$$V_w(\rho, z) = \frac{q}{4\pi\epsilon_0\epsilon_w} \left(\frac{1}{r} + \frac{p}{\sqrt{\rho^2 + (z + h)^2}} - \frac{\epsilon_w\epsilon_\ell}{\epsilon_{w\ell}^2} \sum_{n=1}^{\infty} \frac{p^{n-1}p'^n}{\sqrt{\rho^2 + (z + 2nt + h)^2}} \right) \tag{24}$$

in which $r = \sqrt{\rho^2 + (z - h)^2}$ is the distance from the charge q. The potential in the cytosol due to the same charge q is

$$V_c(\rho, z) = \frac{q\,\epsilon_\ell}{4\pi\epsilon_0\epsilon_{w\ell}\epsilon_{\ell c}} \sum_{n=0}^{\infty} \frac{(pp')^n}{\sqrt{\rho^2 + (z - 2nt - h)^2}} \tag{25}$$

where $\epsilon_{\ell c}$ is the mean relative permittivity $\epsilon_{\ell c} = (\epsilon_\ell + \epsilon_c)/2$.

The first 1000 terms of the series (22), (24) and (25) for the potentials $V_\ell(\rho, z)$, $V_w(\rho, z)$ and $V_c(\rho, z)$ are plotted in figure 2 (in volts) for $\rho = 1$ nm as a function of the height z (nm) above the phospholipid bilayer for a unit charge $q = |e|$ at $(\rho, z) = (0, 0)$ (top curve), $(0, 1)$ (second curve), $(0, 2)$ (third curve) and $(0, 6)$ nm (bottom curve). The lipid bilayer extends from $z = 0$ to $z = -5$ nm, and the cytosol lies below $z = -5$ nm. The relative permittivities were taken to be $\epsilon_w = \epsilon_c = 80$ and $\epsilon_\ell = 2$. Figure 3 plots the potential $V_w(\rho, z)$ in the extracellular region due to a unit charge at the origin as a function of ρ for $z = 0.5$ nm.

In and near the extracellular region, these potentials are fairly well approximated by the simple formulas

$$V_w(\rho, z) \approx \frac{q}{4\pi\epsilon_0\epsilon_w} \left(\frac{1}{r} + \frac{p}{\sqrt{\rho^2 + (z + h)^2}} \right) \tag{26}$$

$$V_\ell(\rho, z) \approx \frac{q}{4\pi\epsilon_0\epsilon_{wl}\, r} \tag{27}$$

which hold when the lipid bilayer is infinitely thick. But the potential drops significantly below this formula (27) as z

descends deeper into the bilayer until it nearly vanishes at the lipid-cytosol interface and in the cytosol. In fact, a charge of $12|e|$ at the origin raises the potential $V_\ell(\rho, z)$ on the interface at $(\rho, z) = (1, -5)$ nm only to 0.0079 V. Thus, the energy advantage of a PS at $(1, -5)$ nm is only 0.0079 eV, which is much less than $kT_b \approx 0.027$ eV. So a CPP on the interface between the lipid bilayer and the extracellular fluid has a very small effect on the PSs of the inner leaflet whose negative charges lie on the lipid–cytosol interface.

It follows that the counterions of the extracellular fluid also have little effect upon the PSs. And since the electric permittivities of the extracellular fluid and of the cytosol are similar, we may view figure 2 upside down and conclude that the PSs and the K^+ and Cl^- ions of the cytosol have little effect upon the CPP and the counterions of the extracellular fluid except to contribute most of the transmembrane potential that exists in the absence of CPPs. Charges in the cytosol are effectively decoupled from those in the extracellular environment.

We may draw a further lesson from the sharp drop in V_ℓ across the lipid bilayer shown in figure 2. The transmembrane potential ΔV due to a CPP on the interface ($z = 0$) is much larger than the simple formula (27) would imply. This is why CPPs are transduced.

4.3. Monte Carlo of the phosphatidylserines

Phosphatidylserines (PSs) make up some 8–18% of the inner leaflet by weight [46]. They diffuse laterally within that leaflet with a diffusion constant $D \approx 10^{-8}$ cm^2 s^{-1} [47] and so within one second spread to an area of 12 μm^2, which is a significant fraction of the surface area of a eukaryotic cell.

My Monte Carlo simulations of the distribution of the PSs of the inner leaflet verified the conclusions of the last subsection (4.2) based upon the analytic potentials (22)–(25) and showed that the PSs are randomly and uniformly distributed, at least to a good approximation. Figure 4 superposes 10 snapshots of the (x, y) locations of 255 PSs in a disk of radius 25 nm that is 5 nm directly below a 12-mer of arginine R^{12}. The snapshots were taken every 2000 sweeps after 25 000 thermalizing sweeps. The 255 PSs moved so as to minimize their free energy due to interactions with the R^{12}, with each other and with the PSs outside the disk. The distribution shows no obvious clustering.

I considered the case of a single CPP of $5 \leqslant N \leqslant 12$ arginines. A CPP of N arginines can form an α-helix of length $L_\alpha \approx 0.16(N-1)$ nm, a random coil of length $L_r \approx 0.25(N-1)$ nm, or a β-strand of length $L_\beta \approx 0.34(N-1)$ nm. The random-coil and β-strand configurations spread the positively charged guanidinium groups farther apart and so would be expected to cluster the PSs even less than the α-helix configuration. So in the simulations of this subsection, I only used the α-helix configuration.

The Monte Carlo code [48] assumes that a PS has a cross-sectional area of 1 nm^2 and that the PSs make up 13% of phospholipids of the inner leaflet. There are then about $0.13\pi R^2$ PSs in a disk of radius R nm, or 255 PSs in a disk of radius 25 nm. The codes allow these 255 PSs to move about within that disk attracted by the electric potential of the N or $2N$ positively charged arginines and repelled by each other and by the PSs outside the disk, which are treated as a uniform surface charge. The computations are facilitated somewhat by the continuity of the electric potentials (22, 24 and 25) across the interfaces at $z = 0$ and $z = -t$ between the lipid bilayer and respectively the extra-cellular medium and the cytosol.

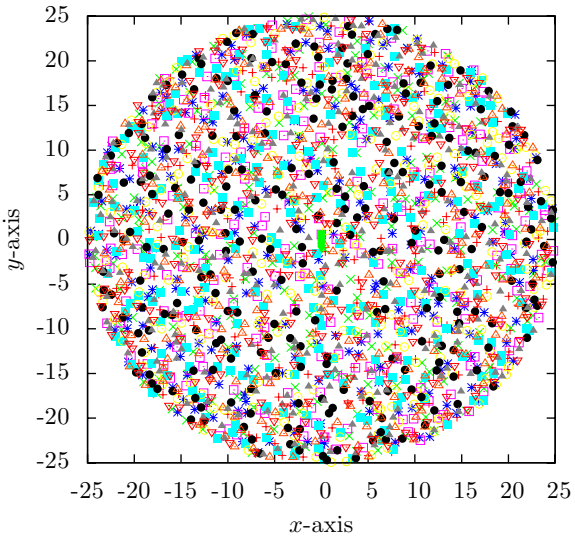

Figure 4. Superposition of 10 plots of the positions $(x, y, -5)$ nm of 255 phosphatidylserines inside a disk of radius 25 nm on the lipid-cytosol interface 5 nm below an α-helix of 12 arginines at $(0, y, 0)$ for $-0.96 \leqslant y \leqslant 0.8$ nm (x's, green). To a good approximation, the PSs are uniformly and randomly distributed.

The code assumes that the N arginines form an alpha helix with positive charges at the points

$$\boldsymbol{r}_{j\mathrm{CPP}} = (0, 0.16(N/2 - j), 0). \tag{28}$$

The PSs were allowed to move in two dimensions within the disk of radius 25 nm in the inner leaflet at sites $\boldsymbol{r}_k$ for $k = 1, \ldots, 255$.

The electrostatic energy of a single PS at the point $\boldsymbol{r}_k$ is the sum of three different energies:

$$E_k = E_{k,\mathrm{CPP}} + E_{k,\mathrm{PSs}} + E_{k,\sigma}. \tag{29}$$

The first energy $E_{k,\mathrm{CPP}}$ is due to its interaction with arginines of the CPP(s)

$$E_{k,\mathrm{CPP}} = \sum_{j=1}^{M} -eV_c(|\boldsymbol{r}_k - \boldsymbol{r}_{j\mathrm{CPP}}|, -t) \tag{30}$$

in which $M = N$ for a single CPP and $M = 2N$ for two CPPs. The second energy $E_{k,\mathrm{PSs}}$ is due to the interaction of the kth PS with the $N_{\mathrm{PS}} - 1 = 254$ other PSs in the disk

$$E_{k,\mathrm{PSs}} = \sum_{k'=1, k' \neq k}^{N_{\mathrm{PS}}} eV_w(|\boldsymbol{r}_k - \boldsymbol{r}_{k'}|, 0). \tag{31}$$

The third energy $E_{k,\sigma}$ is due to the interaction of the kth PS with all the PSs outside the disk represented by a uniform

surface charge $\sigma = 0.13e$ nm^{-2}. In appendix B, I derive the approximation

$$E_{k,\sigma} \approx \frac{\sigma R}{2\epsilon_0\epsilon_w} \sum_{n=1}^{\infty} \frac{1}{2n-1} \left[\frac{(2n)!}{(n!)^2 2^{2n}}\right]^2 \left(\frac{r_k}{R}\right)^{2n} \tag{32}$$

apart from an irrelevant infinite constant. In the computer programs, the upper limit on the summation was $n = 800$.

The Monte Carlo codes use a simple Metropolis step in which the x–y coordinates of a single PS, the kth, are randomly varied by as much as ± 5 nm (to keep the acceptance rate down to 68%). The codes accept any move that lowers the energy E_k as given by (29) and also accept any move that raises E_k by ΔE_k conditionally with the probability

$$P = \mathrm{e}^{-\Delta E_k/(kT_b)} \tag{33}$$

in which k is Boltzmann's constant and T_b is 37 °C. A sweep consists of $k = 1, \ldots, N_{\mathrm{PS}} = 255$ Metropolis steps. Each simulation started from a random configuration of PSs in the disk of radius $R = 25$ nm and ran for 45,000 sweeps. Measurements began after 25 000 sweeps for thermalization.

The radius of an electropore is about $r_p = 1$ nm, and the thickness of the plasma membrane was taken to be $t = 5$ nm. The code measured the electrostatic potential across the lipid bilayer between points that were offset in the x-direction by 1 nm, that is, between the points $(1, 0, 0)$ and $(1, 0, -5)$ nm. The code measured the voltage across the membrane every 10 sweeps and recorded the positions of the PSs every 2000 sweeps.

The transmembrane potential ΔV due to a single α-helix oligoarginine R^N and its cloud of PSs rises with the number of arginines from about $\Delta V = -380$ mV for $N = 5$ arginines to $\Delta V = -630$ mV for $N = 9$ and $\Delta V = -800$ mV for $N = 12$. These voltages are so high that one would have expected electroporation even for R^5s, which is not seen; they are too high because the simulations did not include the Na^+ and Cl^- ions in the extra-cellular medium. The PSs contributed only about 70 mV to the transmembrane potentials.

In all these simulations, the mean value of the distance of the PSs from the point (0, 0, -5) nm was about 17 nm. The distributions of the PSs across the disk of radius $r = 25$ nm appeared uniform and random, with little clustering under the CPPs as shown in figure 4. The reason for the tepid PS response to the electric field of the CPPs can be seen in figure 2: the electric potential $V(\rho, z)$ drops off sharply as z descends through the lipid bilayer and is very small near the lipid–cytosol interface. This uniformity of the PS distribution on the inner leaflet means that we need not simulate their behavior explicitly. We can use the resting transmembrane potential in the absence of CPPs to represent both the PSs and the counterions of the cytosol. Ideally, one should take this ΔV_{cell} from experimental measurements.

4.4. The potential of an oligoarginine

This subsection computes the transmembrane potential ΔV_{CPP} due to an R^n oligoarginine whose n unit positive charges for $5 \leqslant n \leqslant 12$ were fixed at the points

$$\boldsymbol{r}_{j\mathrm{CPP}} = (0, (N/2 - j)\Delta y, 0) \tag{34}$$

Table 2. The voltage differences ΔV_{CPP} (mV) across the plasma membrane due to an R^N oligoarginine as an α-helix, a random coil, or a β-strand. Neither the salt potential ΔV_{NaCl} nor the resting cell potential ΔV_{cell} is included.

N	R^N α-helix	R^N random coil	R^N β-strand
5	−312	−302	−291
6	−376	−362	−346
7	−439	−419	−393
8	−502	−472	−425
9	−562	−521	−455
10	−620	−557	−476
11	−676	−587	−499
12	−729	−614	−516

in which $\Delta y = 0.16$, 0.25 and 0.34 nm respectively for an α-helix, a random coil and a β-strand. I took this ΔV_{CPP} to be the difference

$$\Delta V_{\mathrm{CPP}} = \langle V_c(\rho, -t)\rangle - \langle V_w(\rho, 0)\rangle \tag{35}$$

in which $\langle V_w(\rho, 0)\rangle$ and $\langle V_c(\rho, -t)\rangle$ are the mean values of the R^n's electric potential on two disks of radius $r_p = 1$ nm at $z = 0$ and at $z = -t$.

I used a Monte Carlo code [48] to numerically integrate the appropriate potential V_w or V_c (equations (24 or 25)) over the two disks. The code used a million random points on each of the disks (of which the fraction $(4 - \pi)/4 = 0.215$ were discarded because they lay outside the disk). In this code, I kept 100 terms in the series (24 and 25); the error introduced by this truncation is completely negligible (about 2 parts in 10 million).

The resulting transmembrane potentials ΔV_{CPP} are listed in table 2. The magnitude of ΔV_{CPP} naturally increases with the charge $n|e|$. Because the n charges are more spread out in a β-strand than in a random coil, the magnitude of ΔV_{CPP} is less for a β-strand than for a random coil of the same charge, and similarly for a coil and an α-helix.

4.5. Monte Carlo of the counterions

In this subsection, I use Monte Carlo methods to compute the transmembrane potential ΔV_{NaCl} due to the sodium and chloride ions of the extracellular medium near an oligoarginine.

The Na^+, K^+, Mg^{++}, Ca^{++} and Cl^- concentrations in the extracellular medium respectively are 145, 5, 1–2, 1–2 and 110 mM [49]. I approximated their effects by setting the Na^+ and Cl^- concentrations to 156 mM and ignoring the other ions. I used an active volume that was 10 nm wide and 20 nm long, and that rose from the lipid bilayer to a height of 5 nm. In this active volume of 200 (nm)^3, I put 94 sodium ions and $(94 + n)$ chloride ions so as to make the charge within the active volume neutral.

To prevent the sodium and chloride ions from avoiding the walls and ceiling of the active volume, I surrounded the walls and ceiling of the active volume with a 1000 (nm)^3 5 nm thick passive volume in which I randomly placed 470 Na^+ and 470 Cl^- ions.

The Monte Carlo code [48] used the potential V_w of equation (24) to compute the energy of an individual sodium

or chloride ion in the active volume due to its interaction with all the ions in the active and passive volumes and with the CPP(s) which did not move. The fixed positions (34) of the n charges of the oligoarginine depended upon whether the R^n was configured as an α-helix, a random coil, or a β-strand. The ions in the passive volume also didn't move, retaining their original random positions, which were different in each run. To speed up the computation, I used only the first eight terms in the series (24) for $V_w(\rho, z)$, which introduced an error of about 0.6%.

In order to prevent the Na^+ and Cl^- ions from collapsing into neutral composite particles of infinite negative energy, I added to $V_w(\rho, z)$ the hard core

$$V_{\mathrm{NaCl}}(r) = \frac{e}{4\pi\epsilon_0\epsilon_w}\frac{r_0^{11}}{12r^{12}}. \tag{36}$$

If we keep only the $1/r$ term of $V_w(\rho, z)$, then the potential $V_w + V_{\mathrm{NaCl}}$ is proportional to

$$\frac{r_0^{11}}{12r^{12}} - \frac{1}{r} \tag{37}$$

which has a minimum at $r = r_0$. I took this parameter to be $r_0 = 0.51$ nm which is the location of both the outer maximum of the NaCl-in-water correlation function $g(r)$ and also the outer minimum of the (SCPISM plus SIF) potential energy of Na^+–Cl^- in water [50]. This choice of r_0 allows the Na^+ and Cl^- ions to keep their hydration shells; 97% of them do keep their hydration shells at 100 mM and 25 C [50]. To prevent the chloride ions from falling into the positive charges of the arginines, I added a similar term to the R–Cl potential but used the somewhat larger value of $r_0 = 0.7$ nm to account for the more spread-out charge of the bidentate guanidinium group.

A sodium or chloride ion of charge $q = \pm|e|$ also is subject to an electrostatic potential $V(z)$ that is proportional to the transmembrane voltage ΔV_{cell} reduced by the ratio ϵ_ℓ/ϵ_w of the two permittivities and by the ratio of the height z to the thickness t of the lipid bilayer

$$V(z) = -q\frac{\epsilon_\ell}{\epsilon_w}\frac{z}{t}\Delta V_{\mathrm{cell}}. \tag{38}$$

This energy is small compared to kT_b. Even for $\Delta V_{\mathrm{cell}} = -100$ mV and $z = t$, it is only $kT_b/10$. I used the nominal value of -60 mV for ΔV_{cell} in my simulation of the effect of the salt on the transmembrane potential.

The Monte Carlo code measured the transmembrane potential

$$\Delta V_{\mathrm{NaCl}} = V_{\mathrm{NaCl}}(0, 0, -t) - V_{\mathrm{NaCl}}(0, 0, 0) \tag{39}$$

due to the salt ions of the active volume. It used the first 100 terms of the potential $V_c(\rho, z)$ in the cytosol (25) to compute $V_{\mathrm{NaCl}}(0, 0, -t)$, and it used the first 100 terms of the potential $V_w(\rho, z)$ in the extracellular medium (24) to compute $V_{\mathrm{NaCl}}(0, 0, 0)$. The errors of truncation were negligible.

Each run started by assigning random positions to the 94 Na^+ ions and the $(94+n)$ Cl^- ions of the active volume and to the 470 sodium and 470 chloride ions of the passive volume. After this initialization, the code did 25 000 thermalizing sweeps in which every Na^+ and Cl^- ion of the active volume was allowed to move as much as 1/4th of its range in each direction. After thermalization, the code measured the transmembrane potential every 10 sweeps for a total of 2500 measurements. Five runs were done for each number $5 \leqslant n \leqslant 12$ of arginines. The resulting transmembrane potentials ΔV_{NaCl} due to the salt are listed in mV in table 3.

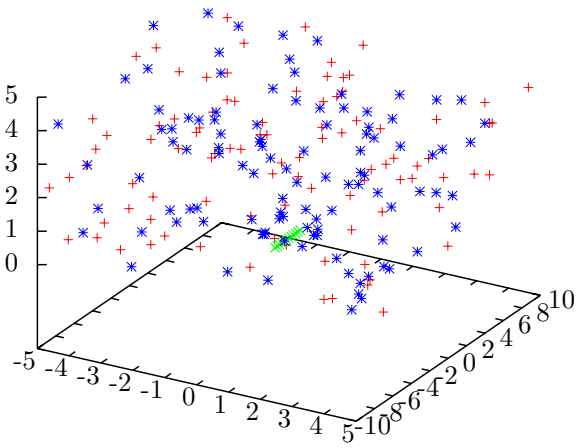

Figure 5. Snapshot of 94 sodium ions (pluses, red), 106 chloride ions (stars, blue) and a 12-mer random coil of oligoarginine R^{12} (x's, green) after 50 000 sweeps. The coordinates are in nm.

Table 3. The voltage differences ΔV_{NaCl} (mV) due to the 156 mM Na^+ and Cl^- ions near an R^N oligoarginine as an α-helix, a random coil, or a β-strand. The resting transmembrane potential ΔV_{cell} is not included, nor ΔV_{CPP} due to the oligoarginine.

N	R^N α-helix	R^N random coil	R^N β-strand
5	168 ± 4	148 ± 3	143 ± 4
6	202 ± 4	189 ± 4	178 ± 1
7	233 ± 4	218 ± 3	204 ± 2
8	270 ± 3	244 ± 1	226 ± 5
9	306 ± 6	275 ± 2	250 ± 4
10	339 ± 2	297 ± 5	266 ± 4
11	370 ± 5	327 ± 3	281 ± 4
12	406 ± 4	353 ± 4	303 ± 2

The code took snapshots of the distributions of the sodium and chloride ions every 2500 sweeps after thermalization. Figure 5 displays the last snapshot (after 50 000 sweeps) of 94 Na^+, 106 Cl^- and 12 Rs in a random coil. The coordinates are in nm.

4.6. Summary of the model

In the present model of CPP transduction, the transmembrane potential is the sum of three terms—the resting transmembrane potential ΔV_{cell} of the cell in the absence of CPPs, the transmembrane potential ΔV_{CPP} due to an oligoarginine, and the transmembrane potential ΔV_{NaCl} due to the counterions of the extracellular medium

$$\Delta V = \Delta V_{\mathrm{cell}} + \Delta V_{\mathrm{CPP}} + \Delta V_{\mathrm{NaCl}}. \tag{40}$$

The dominant term is the one ΔV_{CPP} due to the CPP; it is nearly twice as big as the one ΔV_{NaCl} due to the salt and of opposite sign. The resting transmembrane potential ΔV_{cell} of the cell, which arises mostly from the phosphatidylserines of the inner leaflet, augments the sum $\Delta V_{\mathrm{CPP}} + \Delta V_{\mathrm{NaCl}}$ by some 10–50% depending upon the CPP's charge and the value of ΔV_{cell}.

Table 4. The voltage differences $\Delta V_{CPP} + \Delta V_{NaCl}$ (mV) across the plasma membrane induced by an R^N oligoarginine as an α-helix, a random coil, or a β-strand and by the ions of 156 mM Na^+ and Cl^- reacting to it. The resting transmembrane potential ΔV_{cell} is not included.

N	R^N α-helix	R^N random coil	R^N β-strand
5	-144 ± 4	-154 ± 3	-148 ± 4
6	-174 ± 4	-173 ± 4	-168 ± 1
7	-206 ± 4	-201 ± 3	-189 ± 2
8	-232 ± 3	-228 ± 1	-199 ± 5
9	-256 ± 6	-246 ± 2	-205 ± 4
10	-281 ± 2	-260 ± 5	-210 ± 4
11	-306 ± 5	-260 ± 3	-218 ± 4
12	-323 ± 4	-261 ± 4	-213 ± 2

This salty CPP–PS capacitor increases the transmembrane potential V and so elevates the Boltzmann factor $e^{-E(r)/(kT)}$ and so increases the probability of pore formation—at least for R^Ns with enough arginines. It is hard to be quantitative here because the voltage required to form a pore depends upon the duration of the voltage, the radius of the pore and any defects or fluctuations in the membrane.

In its use of an electric field and of the binding of the CPPs to the phosphate groups of the phospholipids of the outer leaflet, the model has something in common with the adaptive-translocation model of Rothbard, Jessop and Wender [23]; in its invocation of electroporation, it has some overlap with the work of Binder and Lindblom [51]; in its use of neutral dipolar PC & SM head groups it is somewhat similar to the work of Herce and Garcia [52] and of Tang, Waring and Hong [53]. The key distinctive feature of the present model is its underpinning of continuum electrostatics and its quantitative synthesis of the contributions of the CPP, the salt and the phosphatidylserines which combine to form a salty CPP–PS capacitor with a voltage high enough to cause reversible electroporation.

5. Comparison with experiment

5.1. Empirical upper limit on size of cargo

Various groups have found that cell-penetrating peptides cannot transduce cargos of more than about 50 amino acids [18], an upper limit that surely varies with the cell, the CPP and the cargo. In the transduction experiments [4–16] aimed at eventual therapies, the heaviest cargo was 33 amino acids. The present model based on molecular electroporation offers a qualitative explanation for this upper limit.

The masses $M_{N,A}$ of larger cargoes of $A = 50$–100 amino acids of 130 Da each together with N arginines run from $M_{N,A} = 0.16N + 6.5$ to $M_{N,A} = 0.16N + 13$ kDa. Our previous formula (3) gives lower bounds on the radii of such proteins that run from 1.29 to 1.58 nm for CPPs of $N = 10$ arginines. But the energy $E(r)$ of a pore rises with its radius r as shown by equation (19) and so the chance of pore formation falls with the pore radius as shown by figure 1. So the chance of a pore forming that is big enough for a cargo much larger than 50 aa is small. Such cargoes cannot easily fit through the pores that are most likely to form.

Table 5. The fractions of mouse C_2C_{12} myoblasts transduced by oligoarginines L-R^N at three concentrations (μM).

N	10 μM	50 μM	100 μM
5	0.0 ± 0.01	0.0 ± 0.01	0.01 ± 0.01
6	0.0 ± 0.01	0.04 ± 0.03	0.28 ± 0.03
7	0.0 ± 0.01	0.18 ± 0.03	0.75 ± 0.03
8	0.02 ± 0.02	0.31 ± 0.06	0.85 ± 0.04
9	0.05 ± 0.04	0.42 ± 0.10	0.90 ± 0.04
10	0.70 ± 0.04	0.73 ± 0.04	0.91 ± 0.04
11	0.81 ± 0.07	0.83 ± 0.03	0.92 ± 0.04
12	0.90 ± 0.04	0.92 ± 0.02	0.99 ± 0.02

Table 6. The voltage differences ΔV (mV) across the plasma membrane induced by two oligoarginines separated by 2 nm and configured as α-helices or as β-strands. The solution was 156 mM NaCl as in table 4. Includes a resting potential $\Delta V_{cell} = -30$ mV.

N	2 R^N α-helices	2 R^N β-strands
5	-249 ± 3	-238 ± 4
6	-286 ± 7	-271 ± 6
7	-333 ± 5	-284 ± 4
8	-365 ± 6	-295 ± 3
9	-401 ± 11	-304 ± 4
10	-447 ± 3	-308 ± 7
11	-483 ± 2	-310 ± 6
12	-509 ± 5	-308 ± 5

5.2. Experiments with mouse myoblasts

Tünnemann *et al* [31] used confocal laser-scanning microscopy to measure the ability of the L- and D-isoforms of oligolysine and of oligoarginine to carry fluorophores of ~400 Da into live C_2C_{12} mouse myoblasts within 1h. They found that oligoarginines transduced the fluorophores much better than oligolysines and that more arginines meant faster transduction, with L-R9 and L-R10 doing better than their shorter counterparts as shown in table 5. They also found that the D-isoforms worked better than the L-isoforms and that transduction rose with the CPP concentration faster than linearly, which may suggest a cooperative effect.

The present model is consistent with these experimental facts and explains them as follows. The oligoarginines crossed cell membranes more easily than the oligolysines because they were better able to bind to the phosphate groups of the PCs and SMs in the outer leaflet; the oligolysines were not able to form a stable upper plate of a salty CPP–PS capacitor. CPPs with more arginines were transduced more rapidly because with more arginines they could bind to more PCs and SMs and because their higher charges led to higher transmembrane potentials, as noted in table 2. The D-isoforms worked better than the L-isoforms because the capacitor mechanism is insensitive to the chirality of the amino acids and because proteases were less able to cut them. To check for a cooperative effect, I ran some Monte Carlo simulations in which two oligoarginines were as close as 2 nm. In these simulations, I set $r_0 = 0.55$ nm for NaCl and 0.7 nm for R-Gdm. The resulting transmembrane potentials ΔV are listed in table 6 for $\Delta V_{cell} = -30$ mV. They are higher than those due to

a single R^n, which appear in table 4 (even after $\Delta V_{\text{cell}} = -30$ mV is added in). Thus, higher CPP concentrations accelerate transduction because they increase the odds of two or more CPPs attaching to nearly the same spot on the outer leaflet. There is also the *possibility* that under physiological conditions two oligoarginines might form an anti-parallel β-sheet [54]. Such β-sheets would entail a cooperative effect.

This consistency of the capacitor model and its simplicity lends it some plausibility. But evolution finds what works, not what fits neatly into a model, and so other CPPs with different cargos may enter different cells by different mechanisms. In particular, this model may not apply to model amphiphilic peptides (MAPs).

6. Three tests of the model

One way to test the model would be to compare the rates of polyarginine transduction in wild-type cells and in those that have little or no phosphatidylserine (PS) in their plasma membranes. If PS plays a role as in the model of this paper and augments the transmembrane potential by 10–50%, then the transduction of polyarginine fused to a cargo of less than 30 amino acids should be somewhat faster in the wild-type cells than in those without PS in their plasma membranes. Mammalian cell lines that are deficient in the synthesis of phosphatidylserine do exist [55–59], but they appear to have normal levels of PS in their plasma membranes [59]—presumably due to a lower rate of PS degradation [60].

Another test would be to construct artificial asymmetric bilayers [61–63] with and without PS on the 'cytosolic' side and to compare the rates of CPP–cargo transduction. If the present model is right, then the rate of transduction should be somewhat higher through membranes with PS on the cytosolic side than through membranes with no PS or with PS on both sides.

If CPPs do enter cells via molecular electroporation, then it may be possible to observe the formation of transient (<1 ms) pores by detecting changes in the conductance of the membrane [45]. Such measurements would be a key test of the model and, if done on an artificial membrane, would let one determine both whether CPP-transduction is related to the presence of PS on the cytosolic side of the membrane and whether it proceeds via molecular electroporation.

7. Summary

Cell-penetrating peptides (CPPs) can carry into cells cargoes with molecular weights of as much as 3000 Da—much greater than the nominal limit 500 of the 'rule of 5' [64]. Therapeutic applications with well-chosen peptide cargoes of 8–33 amino acids are described in references [4–16].

Section 4 describes a model in which molecular electroporation and phosphatidylserines (PSs) play key roles in the transduction of CPP–cargo molecules. In this model, one or more positively charged CPPs on the outer leaflet and the negatively charged PSs under it on the inner leaflet form a kind of capacitor with a transmembrane potential in excess of 200 mV for a single CPP of nine arginines. This transmembrane potential increases the chance of the formation of electropores through which the CPP and its cargo can enter the cell. The model is consistent with the empirical upper limit on the cargo of about 50 amino acids and with data [31] on how the probability of transduction of polyarginine CPPs into mouse myoblasts depends upon the concentration of the CPP–cargo molecules and the number of arginines in each CPP.

The model predicts that mammalian cells that lack phosphatidylserine in their plasma membranes transduce polycations less well than those that do, that artificial asymmetric bilayers with PS on the cytosolic side transduce polycations better than ones without PS and that the passage of CPPs should be accompanied by transient rises in the conductance of the membrane of the cell or BLM.

Acknowledgments

I am grateful to Leonid Chernomordik for tips about electroporation, to Gisela Tünnemann for sharing her data, to Sergio Hassan for advice about the NaCl potential, to Pavel Jungwirth for advice on guanidinium groups, to John Connor and Karlheinz Hilber for explaining the status of measurements of the membrane potential of mouse myoblast cells, to Paul Robbins for sending me some of his images, and to Jean Vance for information about mammalian cells deficient in the synthesis of phosphatidylserine. Thanks also to H Berg, S Bezrukov, H Bryant, P Cahill, D Cromer, E Evans, B Goldstein, G Herling, T Hess, S Koch, V Madhok, M Malik, A Parsegian, B B Rivers, K Thickman, T Tolley and J Thomas for useful conversations, and to K Dill, S Dowdy, S Henry, K Hilber, A Pasquinelli, B Salzberg, D Sergatskov, L Sillerud, B Smith, A Strongin, R Tsien, J Vance and A Ziegler for helpful e-mails.

Appendix A. First electrostatic problem

Here we derive in the continuum limit the electrostatic potential $V(\rho, \phi, z)$ in cylindrical coordinates due to a charge q on the z-axis at the point $(0, 0, h)$ in the extracellular environment, a height h above the phospholipid bilayer of a eukaryotic cell. The height h is assumed to be less than about 100 nm so that the bilayer can be considered to be flat.

In electrostatic problems, Maxwell's equations reduce to Gauss's law

$$\nabla \cdot \mathbf{D} = \rho \tag{A.1}$$

which relates the divergence of the electric displacement $\mathbf{D}$ to the density ρ of free charges (charges that are free to move in or out of the dielectric medium—as opposed to those that are part of the medium and bound to it by molecular forces), and the static form of Faraday's law

$$\nabla \times \mathbf{E} = 0 \tag{A.2}$$

which implies that the electric field $\mathbf{E}$ is the gradient of an electrostatic potential

$$\mathbf{E} = -\nabla V. \tag{A.3}$$

Across an interface with normal vector $\hat{\mathbf{n}}$ between two dielectrics, the tangential component of the electric field is continuous

$$\hat{\mathbf{n}} \times (\mathbf{E}_2 - \mathbf{E}_1) = 0 \tag{A.4}$$

while the normal component of the electric displacement jumps by the surface density σ of free charge

$$\hat{\mathbf{n}} \cdot (\mathbf{D}_2 - \mathbf{D}_1) = \sigma. \tag{A.5}$$

In a linear dielectric, the electric displacement $\boldsymbol{D}$ is proportional to the electric field $\boldsymbol{E}$

$$\boldsymbol{D} = \epsilon \boldsymbol{E} \tag{A.6}$$

and the coefficient ϵ is the permittivity of the material. The permittivity $\epsilon(m)$ of a material m differs from that of the vacuum ϵ_0 by the electric susceptibility χ and by the relative permittivity ϵ_m:

$$\epsilon(m) = \epsilon_0 + \chi = \epsilon_m \epsilon_0. \tag{A.7}$$

The relative permittivity ϵ_m often is denoted by K_m.

The lipid bilayer is taken to be flat and of a thickness $t \approx 5$ nm. The relative permittivity of the lipid bilayer is $\epsilon_\ell \approx 2$, that of the extra-cellular environment is $\epsilon_w \approx 80$ and that of the cytosol is $\epsilon_c \approx 80$.

We use the method of image charges. The charge q at $(0, 0, h)$ will generate image charges at the points $\boldsymbol{r} = (0, 0, 2nt \pm h)$ in which n runs over all the integers. The cylindrical symmetry of the problem ensures that the potential is independent of the azimuthal angle ϕ and so can depend only upon ρ and z. With $\rho^2 = x^2 + y^2$, the potential in the lipid bilayer is

$$V_\ell(\rho, z) = \frac{1}{4\pi\epsilon_0\epsilon_\ell}\left[\frac{q_0}{\sqrt{\rho^2 + (z-h)^2}} + \sum_{s=\pm1}\sum_{0\neq n=-\infty}^{\infty} \frac{q_{n,s}}{\sqrt{\rho^2 + (z - (2nt + sh))^2}}\right] \tag{A.8}$$

while that in the extracellular environment is

$$V_w(\rho, z) = \frac{1}{4\pi\epsilon_0\epsilon_w}\sum_{s=\pm1}\sum_{n=-\infty}^{0} \frac{q_{wn,s}}{\sqrt{\rho^2 + (z - (2nt + sh))^2}} \tag{A.9}$$

and that in the cytosol is

$$V_c(\rho, z) = \frac{1}{4\pi\epsilon_0\epsilon_c}\sum_{s=\pm1}\sum_{n=0}^{\infty} \frac{q_{cn,s}}{\sqrt{\rho^2 + (z - (2nt + sh))^2}}. \tag{A.10}$$

The continuity (A.4) of the transverse electric field E_ρ and that (A.5) of the normal displacement D_z across the planes $z = 0$ and $z = -t$ implies that the coefficients q_0, $q_{n,s}$, $q_{wn,s}$ and $q_{cn,s}$ must satisfy for $n > 0$ and $s = \pm1$ the relations

$$q_{n,s} + q_{-n,-s} = \frac{\epsilon_\ell}{\epsilon_w} q_{w-n,-s} \tag{A.11}$$

$$q_{n,s} - q_{-n,-s} = -q_{w-n,-s} \tag{A.12}$$

$$q_{n,s} + q_{-(n+1),-s} = \frac{\epsilon_\ell}{\epsilon_c} q_{cn,s} \tag{A.13}$$

$$q_{n,s} - q_{-(n+1),-s} = q_{cn,s} \tag{A.14}$$

as well as the special cases

$$q_{w0,1} + q_{w0,-1} = \frac{\epsilon_w}{\epsilon_\ell} q_0 \tag{A.15}$$

$$q_{w0,1} - q_{w0,-1} = q_0 \tag{A.16}$$

$$q_0 + q_{-1,-1} = \frac{\epsilon_\ell}{\epsilon_c} q_{c0,1} \tag{A.17}$$

$$q_0 - q_{-1,-1} = q_{c0,1} \tag{A.18}$$

$$q_{-1,1} = \frac{\epsilon_\ell}{\epsilon_c} q_{c0,-1} \tag{A.19}$$

$$q_{-1,1} = -q_{c0,-1} \tag{A.20}$$

the last two of which imply that

$$q_{-1,1} = q_{c0,-1} = 0. \tag{A.21}$$

The four equations (A.11)–(A.14) tell us that for $n > 0$ and $s = \pm1$

$$q_{n,s} = -\frac{\epsilon_w - \epsilon_\ell}{2\epsilon_w} q_{w-n,-s} \tag{A.22}$$

$$q_{-n,-s} = \frac{\epsilon_w + \epsilon_\ell}{2\epsilon_w} q_{w-n,-s} \tag{A.23}$$

$$q_{n,s} = \frac{\epsilon_c + \epsilon_\ell}{2\epsilon_c} q_{cn,s} \tag{A.24}$$

$$q_{-(n+1),-s} = -\frac{\epsilon_c - \epsilon_\ell}{2\epsilon_c} q_{cn,s} \tag{A.25}$$

from which we can infer that for $n > 0$

$$q_{n,s} = -p q_{-n,-s} \tag{A.26}$$

and that for $n > 1$ and $s = \pm1$

$$q_{n,s} = (pp')^{n-1} q_{1,s} \tag{A.27}$$

$$q_{-n,s} = -p^{n-2} p'^{n-1} q_{1,-s} \tag{A.28}$$

$$q_{cn,s} = (1 + p')(pp')^{n-1} q_{1,s} \tag{A.29}$$

$$q_{w-n,s} = -(1 + p) p^{n-2} p'^{n-1} q_{1,-s}. \tag{A.30}$$

The four relations (A.15)–(A.19) imply that

$$q_{w0,-1} = p q_{w0,1} \tag{A.31}$$

$$q_0 = (1 - p) q_{w0,1} \tag{A.32}$$

$$q_{c0,1} = (1 - p)(1 + p') q_{w0,1} \tag{A.33}$$

$$q_{-1,-1} = -(1 - p) p' q_{w0,1}. \tag{A.34}$$

Gauss's law (A.1) applied to a tiny sphere about the physical charge q gives

$$q_{w0,1} = q. \tag{A.35}$$

This identification and the four equations (A.31)–(A.34) tell us that

$$q_{w0,-1} = pq \tag{A.36}$$

$$q_0 = (1 - p) q \tag{A.37}$$

$$q_{c0,1} = (1 - p)(1 + p') q \tag{A.38}$$

$$q_{-1,-1} = -(1 - p) p' q. \tag{A.39}$$

Equations (A.26)–(A.39) allow us to relate all the coefficients for $n > 0$ to $q_{w0,1} = q$ and to $q_{1,-1} = q_{-1,1} = 0$:

$$q_{n,1} = (pp')^n(1-p)q \tag{A.40}$$
$$q_{n,-1} = (pp')^{n-1}q_{1,-1} = 0 \tag{A.41}$$
$$q_{-n,1} = -p^{n-2}p'^{n-1}q_{1,-1} = 0 \tag{A.42}$$
$$q_{-n,-1} = -p^{n-1}p'^{n}(1-p)q \tag{A.43}$$
$$q_{w-n,1} = -(1+p)p^{n-2}p'^{n-1}q_{1,-1} = 0 \tag{A.44}$$
$$q_{w-n,-1} = -(1-p^2)p^{n-1}p'^{n}q \tag{A.45}$$
$$q_{cn,1} = (1-p)(1+p')(pp')^n q \tag{A.46}$$
$$q_{cn,-1} = (1+p')(pp')^{n-1}q_{1,-1} = 0. \tag{A.47}$$

The electric potential due to a charge q in the extra-cellular environment, a distance h above a lipid bilayer of thickness t then is

$$V_\ell(\rho,z) = \frac{q}{4\pi\epsilon_0\epsilon_{w\ell}}\sum_{n=0}^{\infty}(pp')^n\left(\frac{1}{\sqrt{\rho^2+(z-2nt-h)^2}} - \frac{p'}{\sqrt{\rho^2+(z+2(n+1)t+h)^2}}\right) \tag{A.48}$$

in the lipid bilayer. That in the extra-cellular environment is

$$V_w(\rho,z) = \frac{q}{4\pi\epsilon_0\epsilon_w}\left(\frac{1}{r} + \frac{p}{\sqrt{\rho^2+(z+h)^2}} - \frac{\epsilon_w\epsilon_\ell}{\epsilon_{w\ell}^2}\sum_{n=1}^{\infty}\frac{p^{n-1}p'^{n}}{\sqrt{\rho^2+(z+2nt+h)^2}}\right) \tag{A.49}$$

in which r is the distance from the charge q. Finally, the potential in the cytosol is

$$V_c(\rho,z) = \frac{q\,\epsilon_\ell}{4\pi\epsilon_0\epsilon_{w\ell}\epsilon_{\ell c}}\sum_{n=0}^{\infty}\frac{(pp')^n}{\sqrt{\rho^2+(z-2nt-h)^2}}. \tag{A.50}$$

Appendix B. Second electrostatic problem

Here I approximate the electrostatic potential $V_\sigma(\boldsymbol{r}_k)$ within a disk of radius R due to a uniform charge density σ of phosphatidylserines (PSs) outside the disk.

The negative charges of the PSs are taken to lie on the interface between the cytosol and the lipid bilayer. The role of this potential V_σ is only to keep the mutual repulsion of the PSs inside the disk from driving them too much toward the perimeter of the disk. So an exact expression for V_σ is not needed. Any formula for it will involve an integral of σ over distances that run to infinity. My approximation is to set the thickness t of the bilayer equal to zero. In this limit, the effective potential felt by a PS at $\boldsymbol{r}_k$ is

$$V_\sigma(\boldsymbol{r}_k) = \sigma\int_R^\infty \mathrm{d}\rho\int_0^{2\pi}\mathrm{d}\phi\;\frac{\rho}{q}\,V_{ws}(|\boldsymbol{\rho}-\boldsymbol{r}_k|) \tag{B.1}$$

in which $\boldsymbol{\rho} = \rho(\cos\phi,\sin\phi,0)$, and $V_{ws}(|\boldsymbol{\rho}-\boldsymbol{r}_k|)$ is the potential $V_w(\rho,z)$ of equation (A.49) for $z=h=t=0$

$$V_{ws}(|\boldsymbol{\rho}-\boldsymbol{r}_k|) = \frac{q}{4\pi\epsilon_0\epsilon_{wc}|\boldsymbol{\rho}-\boldsymbol{r}_k|} \tag{B.2}$$

where $\epsilon_{wc} = (\epsilon_w+\epsilon_c)/2$. With this approximation and with $\epsilon_w \approx \epsilon_c \approx 80$, the potential (B.1) is

$$\begin{aligned} V_\sigma(\boldsymbol{r}_k) &\approx \sigma\int_R^\infty \mathrm{d}\rho\int_0^{2\pi}\mathrm{d}\phi\;\frac{\rho}{4\pi\epsilon_0\epsilon_w|\boldsymbol{\rho}-\boldsymbol{r}_k|} \\ &= \frac{\sigma}{4\pi\epsilon_0\epsilon_w}\int_R^\infty \mathrm{d}\rho\int_0^{2\pi}\mathrm{d}\phi\;\frac{\rho}{\sqrt{\rho^2+r_k^2-2\rho r_k\cos\phi}} \\ &= \frac{\sigma}{4\pi\epsilon_0\epsilon_w}\int_R^\infty \mathrm{d}\rho\int_0^{2\pi}\mathrm{d}\phi\sum_{n=0}^{\infty}\left(\frac{r_k}{\rho}\right)^n P_n(\cos\phi). \end{aligned} \tag{B.3}$$

The $n=0$ term in this sum is an infinite constant, which we drop because it does not affect the containment of the PSs within the disk. The remaining terms are

$$\begin{aligned} V_\sigma(\boldsymbol{r}_k) &\approx \frac{\sigma}{4\pi\epsilon_0\epsilon_w}\int_R^\infty \mathrm{d}\rho\sum_{n=1}^{\infty}\left(\frac{r_k}{\rho}\right)^{2n} 2\pi\left[\binom{2n}{n}2^{-2n}\right]^2 \\ &= \frac{\sigma R}{2\epsilon_0\epsilon_w}\sum_{n=1}^{\infty}\frac{1}{2n-1}\left[\frac{(2n)!}{(n!)^2 2^{2n}}\right]^2\left(\frac{r_k}{R}\right)^{2n}. \end{aligned} \tag{B.4}$$

References

[1] Green M and Loewenstein P M 1988 Autonomous functional domains of chemically synthesized human immunodeficiency virus tat *trans*-activator protein *Cell* **55** 1179–88

[2] Frankel A D and Pabo C O 1988 Cellular uptake of the tat protein from human immunodeficiency virus *Cell* **55** 1189–93

[3] Lindberg M, Jarvet J, Langel Ü and Gräslund 2001 Secondary structure and position of the cell-penetrating peptide transportan in SDS micelles as determined by NMR *Biochemistry* **40** 3141–9

[4] Jiang T, Olson E S, Nguyen Q T, Roy M, Jennings P A and Tsien R Y 2004 Tumor imaging by means of proteolytic activation of cell-penetrating peptides *Proc. Natl Acad. Sci.* **101** 17867–72

[5] Snyder E, Saenz C, Denicourt C, Meade B, Cui X, Kaplan I and Dowdy S 2005 Enhanced targeting and killing of tumor cells expressing the CXC chemokine receptor 4 by transducible anticancer peptides *Cancer Res.* **65** 10646–50

[6] Willam C, Masson N, Tian Y-M, Mahmood S A, Wilson M I, Bicknell R, Eckardt K-U, Maxwell P H, Ratcliffe P J and Pugh C W 2002 Peptide blockade of HIFα degradation modulates cellular metabolism and angiogenesis *Proc. Natl Acad. Sci.* **99** 10423–8

[7] Chen, P. Y-N, Sharma S K, Ramsey T M, Jiang L, Martin M S, Baker K, Adams P D, Bair K W and Kaelin W G Jr 1999 Selective killing of transformed cells by cyclin/cyclin-dependent kinase 2 antagonists *Proc. Natl Acad. Sci.* **96** 4325–9

[8] Mendoza N, Fong S, Marsters J, Koeppen H, Schwall R and Wickramasinghe D 2003 Selective cyclin-dependent kinase 2/Cyclin a antagonists that differ from ATP site inhibitors block tumor growth *Cancer Res.* **63** 1020–4

[9] Harbour J W, Worley L, Ma D and Cohen M 2002 Transducible peptide therapy for uveal melanoma and retinoblastoma *Arch. Ophthalmol.* **120** 1341–6

[10] Mai J C, Mi Z, Kim S-H, Ng B and Robbins P D 2001 A proapoptotic peptide for the treatment of solid tumors *Cancer Res.* **61** 7709–12

[11] Datta K, Sundberg C, Karumanchi S A and Mukhopadhyay D 2001 The 104–123 amino acid sequence of the β-domain of von Hippel-Lindau gene product is sufficient to inhibit renal tumor growth and invasion *Cancer Res.* **61** 1768–75

[12] Hosotani R, Miyamoto Y, Fujimoto K, Doi R, Otaka A, Fujii N and Imamura M 2002 Trojan p16 peptide suppresses pancreatic cancer growth and prolongs survival in mice *Clin. Cancer Res.* **8** 1271–6

[13] Zhou J, Fan J and Hsieh J-T 2006 Inhibition of mitogen-elicited signal transduction and growth in prostate cancer with a small peptide derived from the functional domain of DOC-2/DAB2 delivered by a unique vehicle *Cancer Res.* **66** 8954–8

[14] Snyder E, Meade B, Saenz C and Dowdy S 2004 Treatment of terminal peritoneal carcinomatosis by a transducible p53-activating peptide *PLoS Biology* **2** 0186–93

[15] Haase H *et al* 2006 Minigenes encoding N-terminal domains of human cardiac myosin light chain-1 improve heart function of transgenic rats *FASEB J.* **20** 865–73

[16] Tünnemann G, Karczewski P, Haase H, Cardoso M C and Morano I 2007 Modulation of muscle contraction by a cell-permeable peptide *J. Mol. Med.* **85** 1405–12

[17] Ziegler A and Seelig J 2007 High affinity of the cell-penetrating peptide HIV-1 Tat-PTD for DNA *Biochemistry* **46** 8138–45

[18] Tünnemann G, Martin R M, Haupt S, Patsch C, Edenhofer F and Cardoso M C 2006 Cargo-dependent mode of uptake and bioavailability of TAT-containing proteins and peptides in living cells *FASEB J.* **20** 1775–84

[19] Wadia J S, Stan R V and Dowdy S F 2004 Transducible TAT-HA fusogenic peptide enhances escape of TAT-fusion proteins after lipid raft macropinocytosis *Nat. Med.* **10** 310–5

[20] Duchardt F, Fotin-Mleczek M, Schwarz H, Fischer R and Brock R 2007 A comprehensive model for the cellular uptake of cationic cell-penetrating peptides *Traffic* **8** 848–66

[21] Prochiantz A 2000 Messenger proteins: homeoproteins, TAT and others *Curr. Opin. Cell Biol.* **12** 400–6

[22] Dom G, Shaw-Jackson C, Matis C, Bouffioux O, Picard J J, Prochiantz A, Mingeot-Leclercq M-P, Brasseur R and Rezsohazy R 2003 Cellular uptake of antennapedia penetratin peptides is a two-step process in which phase transfer precedes a tryptophan-dependent translocation *Nucleic. Acids Res.* **31** 556–61

[23] Rothbard J B, Jessop T C and Wender P A 2005 Adaptive translocation: The role of hydrogen bonding and membrane potential in the uptake of guanidinium-rich transporters into cells *Adv. Drug Delivery Rev.* **57** 495–504

[24] Zaro J L and Shen W-C 2005 Evidence that membrane transduction of oligoarginine does not require vesicle formation *Exp. Cell Res.* **307** 164–73

[25] Ziegler A, Nervi P, Dürrenberger M and Seelig J 2005 The cationic cell-penetrating peptide CPP^{TAT} derived from the HIV-1 protein TAT is rapidly transported into living fibroblasts: optical, biophysical, and metabolic evidence *Biochemistry* **44** 138–48

[26] Patel L N, Zaro J L and Shen W-C 2007 Cell penetrating peptides: Intracellular pathways and pharmaceutical perspectives *Pharm. Res.* **24** 1977–92

[27] Fawell S, Seery J, Daikh Y, Moore C, Chen L, Pepinsky B and Barsoum J 1994 Tat-mediated delivery of heterologous proteins into cells *Proc. Natl Acad. Sci.* **91** 664

[28] Nagahara H, Vocero-Akbani A, Snyder E, Ho A, Latham D, Lissy N, Becker-Hapak M, Ezhevsky S and Dowdy S 1998 Transduction of full-length TAT fusion proteins into mammalian cells: $TAT\text{-}p27^{Kip1}$ *Nat. Med.* **4** 1449

[29] Bulte J W 2006 Intracellular endosomal magnetic labeling of cells *Methods in Mol. Med.* **124** 419

[30] Garden O, Reynolds P, Yates J, Larkman D, Marelli-Berg F, Haskard D, Edwards A and George A 2006 A rapid method for labelling $CD4^+$ T cells with ultrasmall paramagnetic iron oxide nanoparticles for magnetic resonance imaging that preserves proliferative, regulatory and migratory behaviour *in vitro J. Immunol. Methods* **314** 123–33

[31] Tünnemann G, Ter-Avetisyan G, Martin R M, Stöckl M, Herrmann A and Cardoso M C 2008 Live-cell analysis of cell penetration ability and toxicity of oligo-arginines *J. Peptide Science* **14** 469–76

[32] Bevers E, Comfurius P, Dekkers D and Zwaal R 1999 Lipid translocation across the plasma membrane of mammalian cells *Biochim. Biophys. Acta* **1439** 317–30

[33] Alberts B, Johnson A, Lewis J, Raff M, Roberts K and Walter P 2002 *Molecular Biology of the Cell* 4th edn (New York: Garland Science) pp 587–93

[34] Vaara M 1992 Agents that increase the permeability of the outer membrane *Microbiol. Rev.* **56** 395–411

[35] Brogden K A 2005 Antimicrobial peptides: pore formers or metabolic inhibitors in bacteria? *Nat. Rev. Microbiol.* **3** 238–50

[36] Tyagi M, Rusnati M, Presta M and Giacca M 2001 Internalization of HIV-1 Tat requires cell surface heparan sulfate proteoglycans *J. Biol. Chem.* **276** 3254–61

[37] Parsegian A 1969 Energy of an ion crossing a low dielectric membrane: solutions to four relevant electrostatic problems *Nature* **221** 844–6

[38] Fischer H, Polikarpov I and Craievich A F 2004 Average protein density is a molecular-weight-dependent function *Protein Sci.* **13** 2825–8

[39] Alberts B, Johnson A, Lewis J, Raff M, Roberts K and Walter P 2008 *Molecular Biology of the Cell* 5th edn (New York: Garland Science) p 620

[40] Dai J, Ting-Beall H P and Sheetz M P 1997 The secretion-coupled endocytosis correlates with membrane tension changes in RBL 2H3 cells *J. Gen. Physiol.* **110** 1–10

[41] Abidor I G, Arakelyan V B, Chernomordik L V, Chizmadzhev Y A, Pastushenko V F and Tarasevich M R 1979 Electric breakdown of bilayer lipid membranes I. The main experimental facts and their qualitative discussion *Bioelectrochem. Bioenerg.* **6** 37–52

[42] Chernomordik L V, Sukharev S I, Popov S V, Pastushenko V F, Sokirko A V, Abidor I G and Chizmadzhev Y A 1987 The electrical breakdown of cell and lipid membranes: the similarity of phenomenologies *Bioch. Biophys. Acta* **902** 360–73

[43] Glaser R W, Leikin S L, Chernomordik L V, Pastushenko V F and Sokirko A V 1988 Reversible electrical breakdown of lipid bilayers: formation and evolution of pores *Bioch. Biophys. Acta* **940** 275–87

[44] Weaver J and Chizmadzhev Y 1996 Theory of electroporation: a review *Bioelectrochem. Bioenerg.* **41** 135–60

[45] Melikov K C, Frolov V A, Shcherbakov A, Samsonov A V, Chizmadzhev Y A and Chernomordik L V 2001 Voltage-induced nonconductive pre-pores and metastable single pores in unmodified planar lipid bilayers *Biophys. J.* **80** 1829–36

[46] Alberts B, Johnson A, Lewis J, Raff M, Roberts K and Walter P 2008 *Molecular Biology of the Cell* 5th edn (New York: Garland Science) p 624

[47] Alberts B, Johnson A, Lewis J, Raff M, Roberts K and Walter P 2008 *Molecular Biology of the Cell* 5th edn (New York: Garland Science) p 622

[48] Cahill K Fortran 90 codes for this paper http://bio.phys.unm.edu/cpp/index.html

[49] Alberts B, Johnson A, Lewis J, Raff M, Roberts K and Walter P 2008 *Molecular Biology of the Cell* 5th edn (New York: Garland Science) p 652

[50] Hassan S A 2008 Computer simulation of ion cluster speciation in concentrated aqueous solutions of ambient conditions *J. Phys. Chem.* B **112** 10573–84
[51] Binder H and Lindblom G 2003 Charge-dependent translocation of the trojan peptide penetratin across lipid membranes *Biophys. J.* **85** 982–95
[52] Herce H D and Garcia A E 2007 Molecular dynamics simulations suggest a mechanism for translocation of the HIV-1 TAT peptide across lipid membranes *Proc. Natl Acad. Sci.* **104** 20805–10
[53] Tang M, Waring A J and Hong M 2007 Phosphate-mediated arginine insertion into lipid membranes and pore formation by a cationic membrane peptide from solid-state NMR *J. Am. Chem. Soc.* **129** 11438–46
[54] Vondrášek J, Mason P, Heyda J, Collins K and Jungwirth P 2009 The molecular origin of like-charge arginine-arginine pairing in water *J. Phys. Chem. B Lett.* **113** 9041–5
[55] Voelker D and Frazier J 1986 Isolation and characterization of a Chinese hamster ovary cell line requiring ethanolamine or phosphatidylserine for growth and exhibiting defective phosphatidylserine synthase activity *J. Biol. Chem.* **261** 1002–8
[56] Kuge O, Saito K, Kojima M, Akamatsu Y and Nishijima M 1996 Post-translational processing of the phosphatidylserine decarboxylase gene product in Chinese hamster ovary cells *Biochem. J.* **319** 33–8
[57] Saito K, Nishijima M and Kuge O 1998 Genetic evidence that phosphatidylserine synthase II catalyzes the conversion of phosphatidylethanolamine to phosphatidylserine in Chinese hamster ovary cells *J. Bio. Chem.* **273** 17199–205
[58] Stone S J and Vance J E 2000 Phosphatidylserine synthase-1 and -2 are localized to mitochondria-associated membranes *J. Biol. Chem.* **275** 34534–40
[59] Grandmaison P A, Nanowski T S and Vance J E 2004 Externalization of phosphatidylserine during apoptosis does not specifically require either isoform of phosphatidylserine synthase *Biochim. Biophys. Acta* **1636** 1–11
[60] Vance J E 2008 private communication
[61] Hanke M and Schlue W-R 1993 *Planar Lipid Bilayers* (New York: Academic)
[62] Rostovtseva T K, Aguilella V M, Vodyanoy I, Bezrukov S M and Parsegian V A 1998 Membrane surface-charge titration probed by Gramicidin a channel conductance *Biophys. J.* **75** 1783–92
[63] O'Shaughnessy T J, Hu J E, Kulp J L III, Daly S M and Ligler F S 2007 Laser ablation of micropores for formation of artificial planar lipid bilayers *Biomed. Microdevices* **9** 863–8
[64] Lipinski C, Lombardo F, Dominy B and Feeney P 1997 Experimental and computational approaches to estimate solubility and permeability in drug discovery and development settings *Adv. Drug Deliv. Rev.* **23** 3–25